CORRECTED 4 DECEMBER 2009; SEE LAST PAGE

An Argonaute Transports siRNAs from the Cytoplasm to the Nucleus

Shouhong Guang,[1]* Aaron F. Bochner,[1,2]* Derek M. Pavelec,[1,3] Kirk B. Burkhart,[1,4] Sandra Harding,[1] Jennifer Lachowiec,[1] Scott Kennedy[1]†

Ribonucleoprotein complexes consisting of Argonaute-like proteins and small regulatory RNAs function in a wide range of biological processes. Many of these small regulatory RNAs are predicted to act, at least in part, within the nucleus. We conducted a genetic screen to identify factors essential for RNA interference (RNAi) in nuclei of *Caenorhabditis elegans* and identified the Argonaute protein NRDE-3. In the absence of small interfering RNAs (siRNAs), NRDE-3 resides in the cytoplasm. NRDE-3 binds siRNAs generated by RNA-dependent RNA polymerases acting on messenger RNA templates in the cytoplasm and redistributes to the nucleus. Nuclear redistribution of NRDE-3 requires a functional nuclear localization signal, is required for nuclear RNAi, and results in NRDE-3 association with nuclear-localized nascent transcripts. Thus, specific Argonaute proteins can transport specific classes of small regulatory RNAs to distinct cellular compartments to regulate gene expression.

To identify factors specifically required for RNA interference (RNAi) in *Caenorhabditis elegans* nuclei, we chemically mutagenized worms and screened for mutant animals that failed to silence nuclear-localized RNAs in response to RNAi, but retained the ability to silence RNAs not localized exclusively in the nucleus (for details see fig. S1) (*1*). We identified 55 mutant alleles that were categorized into three complementation groups. Forty-six of these alleles defined a gene that we termed *nuclear RNAi defective-3* (*nrde-3*). We mapped *nrde-3* to a <1-centimorgan (cM) interval. Open reading frame (ORF) R04A9.2 lies within this genetic interval. R04A9.2 is predicted to encode an Argonaute-like protein containing a bipartite nuclear localization signal (NLS), and a PAZ and a PIWI domain. The PIWI domain of R04A9.2 lacks the DDH catalytic triad of amino acids considered necessary for Argonaute-based Slicer activity: The synonymous residues are EVQ in R04A9.2 (*2*, *3*). Sequencing of R04A9.2 from eight independent *nrde-3* alleles identified seven mutations in R04A9.2 coding sequences (Fig. 1A). Three alleles are predicted to stop translation upstream of the PAZ and PIWI domains of R04A9.2 and, thus, are likely to reveal the null phenotype. Transformation of wild-type R04A9.2 DNA into *nrde-3* mutant animals rescued phenotypes associated with *nrde-3* mutant animals (see below). Thus, R04A9.2 corresponds to *nrde-3*.

A fusion gene of green fluorescent protein (GFP) and full-length NRDE-3 under control of the endogenous *nrde-3* promoter (*1*) rescued *nrde-3* mutant phenotypes, was expressed in most somatic cells after the ~80-cell stage of development, and localized predominantly to the nucleus (Fig. 1B and fig. S2). Immunoprecipitation of NRDE-3 and isolation of coprecipitating RNAs allowed us to clone 465 RNAs of approximately 20 to 22 nucleotides that associated with NRDE-3 in vivo. These RNAs represent endogenous (endo) small interfering RNAs (siRNAs); they map to similar chromosomal loci as previously identified endo siRNAs (table S1). Endo siRNAs are thought to mediate, or to be the consequence of, ongoing negative regulation of endogenously expressed RNAs by RNAi (*4*, *5*). In *eri-1*$^{-}$, *ergo-1*$^{-}$, *mut-7*$^{-}$, *rde-4*$^{-}$, or *mut-2*$^{-}$ animals, which exhibit defects in endo siRNA production (*4*, *5*), NRDE-3 failed to associate with endo siRNAs (*1*) (Fig. 1B). In these mutant backgrounds, NRDE-3 localized to the cytoplasm, which suggests that siRNAs are necessary to localize NRDE-3 to the nucleus (Fig. 1B).

To examine this possibility, we mutated residues within the NRDE-3 PAZ domain (Y463A, Y464A) known to be necessary for siRNA-binding in related Argonaute proteins [termed NRDE-3(*PAZ)] (*6*, *7*). NRDE-3(*PAZ) failed to interact with siRNAs and localized predominantly to the cytoplasm (Fig. 1C). Exposure of animals lacking endo siRNAs (due to loss of ERI-1 activity) to exogenous double-stranded RNA (dsRNA) caused NRDE-3 to relocalize to the nucleus and induced association of NRDE-3 with exogenous (exo) siRNAs (Fig. 1D). The nuclear redistribution of NRDE-3 required NRDE-3–siRNA interactions: NRDE-3(*PAZ) failed to localize to the nucleus in response to dsRNA treatment, and NRDE-3 relocalization was dependent on RDE-4, a dsRNA binding protein necessary for converting experimentally introduced dsRNAs to exo siRNAs (*8*) (Fig. 1D). We conclude that NRDE-3–siRNA binding is necessary and sufficient for NRDE-3 nuclear redistribution.

NRDE-3 is essential for silencing nuclear-localized RNAs. A *pes-10::GFP* transgene expresses a transcript that, for unknown reasons, accumulates in the nucleus during early (<16-cell) embryogenesis. RNAi targeting the *pes-10::GFP* transcript triggered a NRDE-3–dependent loss of nuclear-localized *pes-10::GFP* RNA (*9*) (Fig. 2A and fig. S3). NRDE-3 is also required for RNAi of endogenous nuclear-localized RNAs. The *lin-15b* and *lin-15a* genes are transcribed as a bicistronic pre-mRNA that is spliced within the nucleus into distinct *lin-15b* and *lin-15a* mRNAs (*10*). Animals harboring mutations in both *lin-15b* and *lin-15a*, but not either gene alone, exhibit a multivulva (Muv) phenotype (*11*, *12*). RNAi targeting *lin-15b* results in a low percentage of ani-

[1]Department of Pharmacology, University of Wisconsin–Madison, Madison, WI 53706, USA. [2]Program in Cellular and Molecular Biology, University of Wisconsin–Madison, Madison, WI 53706, USA. [3]Program in Molecular and Cellular Pharmacology, University of Wisconsin–Madison, Madison, WI 53706, USA. [4]Department of Genetics, University of Wisconsin–Madison, Madison, WI 53706, USA.

*These authors contributed equally to this work.
†To whom correspondence should be addressed. E-mail: sgkennedy@wisc.edu

Table 1. NRDE-3 preferentially targets nuclear-localized RNAs. Animals of the indicated genotypes were fed bacteria expressing indicated dsRNAs (e.g., *unc-22*). Phenotypes (e.g., twitcher) of *eri-1(mg366)* animals exposed to control or dsRNA were defined as 0 and 4, respectively (n = 3, ± SD). NS, not scored. Asterisk indicates phenotype predicted to be elicited by silencing of nuclear-localized RNA.

	dsRNA (phenotype scored)						
Genotype	*unc-22* (twitcher)	*unc-15* (paralysis)	*pos-1* (lethality)	*unc-73* (paralysis)	*dpy-13* (dumpy)	*lir-1* (lethality*)	*lin-15b* (multivulva*)
eri-1(mg366)	3.9 ± 0.2	4	3.8 ± 0.4	3.9 ± 0.2	3.9 ± 0.1	4	4
eri-1(mg366);nrde-3(gg066)	3.7 ± 0.4	3	4	1.6 ± 0.8	1.8 ± 0.4	0	0
eri-1(mg366);rde-1(ne219)	0	0	0	0	0	0	0
eri-1(mg366);rde-4(ne301)	0	0	0	0	0	0	0
eri-1(mg366);rrf-1(pk1417)	0	NS	4	0	NS	0	0†

†n = 1.

mals exhibiting a Muv phenotype, consistent with nuclear silencing of the *lin-15* bicistron (*9*). To sensitize this assay, we repeated these experiments in a strain of *C. elegans* (*eri-1*$^{-}$) that exhibits enhanced sensitivity to dsRNAs (*13*). Of *eri-1*$^{-}$ animals exposed to dsRNA targeting *lin-15b*, 95 ± 4% exhibited a Muv phenotype, supporting the hypothesis that nuclear-localized *lin-15* bicistronic RNA can be targeted by RNAi (Table 1). Consistent with these results, RNAi targeting *lin-15b* in *eri-1*$^{-}$ animals triggered a decrease in both *lin-15b* and *lin-15a* pre-mRNA abundance (Fig. 2B). These effects were also observed in wild-type animals but were less pronounced than in *eri-1*$^{-}$ animals. NRDE-3 is required for these phenomena; in response to *lin-15b* RNAi, *eri-1*$^{-}$;*nrde-3*$^{-}$ animals did not exhibit a Muv phenotype (Table 1) and failed to silence the *lin-15b* and *lin-15a* pre-mRNAs (Fig. 2B). NRDE-3–dependent silencing of *lin-15b* pre-mRNA accounted for ~80% of total *lin-15b* silencing elicited by *lin-15b* RNAi (Fig. 2B). Finally, we, and others, have detected RNAi-triggered silencing of nuclear-localized *lir-1–lin-26* polycistronic RNA (*1*, *14*). NRDE-3 is required for this silencing (Table 1). We conclude that NRDE-3 is required for silencing of many, if not all, nuclear-localized RNAs.

Of the 465 NRDE-3–associated endo siRNAs, 33 exhibited sequence complementarity to the E01G4.5 ORF (table S1). Northern blot analysis confirmed that NRDE-3 interacts, in vivo, with E01G4.5 endo siRNAs (fig. S4). *nrde-3*$^{-}$ animals expressed E01G4.5 endo siRNAs at approximately wild-type levels (Fig. 2C). The E01G4.5 pre-mRNA and mRNA, however, were up-regulated four to five times in *nrde-3*$^{-}$ animals (Fig. 2D). *eri-1*$^{-}$ animals [which failed to express E01G4.5 siRNAs (Fig. 2C)] exhibited a similar misregulation of the E01G4.5 pre-mRNA, but a more dramatic (24 times) up-regulation of the E01G4.5 mRNA (Fig. 2D). These data suggest that NRDE-3 represents the primary, if not the sole, means for endogenous silencing of the E01G4.5 pre-mRNA, but other, NRDE-3–independent, mechanisms exist for silencing E01G4.5 mRNA. Thus, NRDE-3 is required for silencing of an endogenous, nuclear-localized RNA and likely functions downstream of endo siRNA production in these silencing events.

We investigated whether silencing in the nucleus is dependent on nuclear localization of NRDE-3. NRDE-3 harboring a three–amino acid substitution (K80A, R81A, K82A) within the predicted NRDE-3 NLS [termed NRDE-3(*NLS)] localized to the cytoplasm (Fig. 3A). Wild-type NRDE-3, but not NRDE-3(*NLS), rescued a Nrde phenotype associated with *nrde-3*$^{-}$ animals (Fig. 3B). Introduction of a heterologous simian virus 40 (SV40) NLS to NRDE-3(*NLS) restored NRDE-3^{+} function and nuclear localization to NRDE-3(*NLS) (Fig. 3, A and B). Thus, NRDE-3 contains a functional NLS, and NRDE-3 must localize to the nucleus to trigger nuclear RNAi. NRDE-3(*NLS), which localized to the cytoplasm, associated with siRNAs to an extent sim-

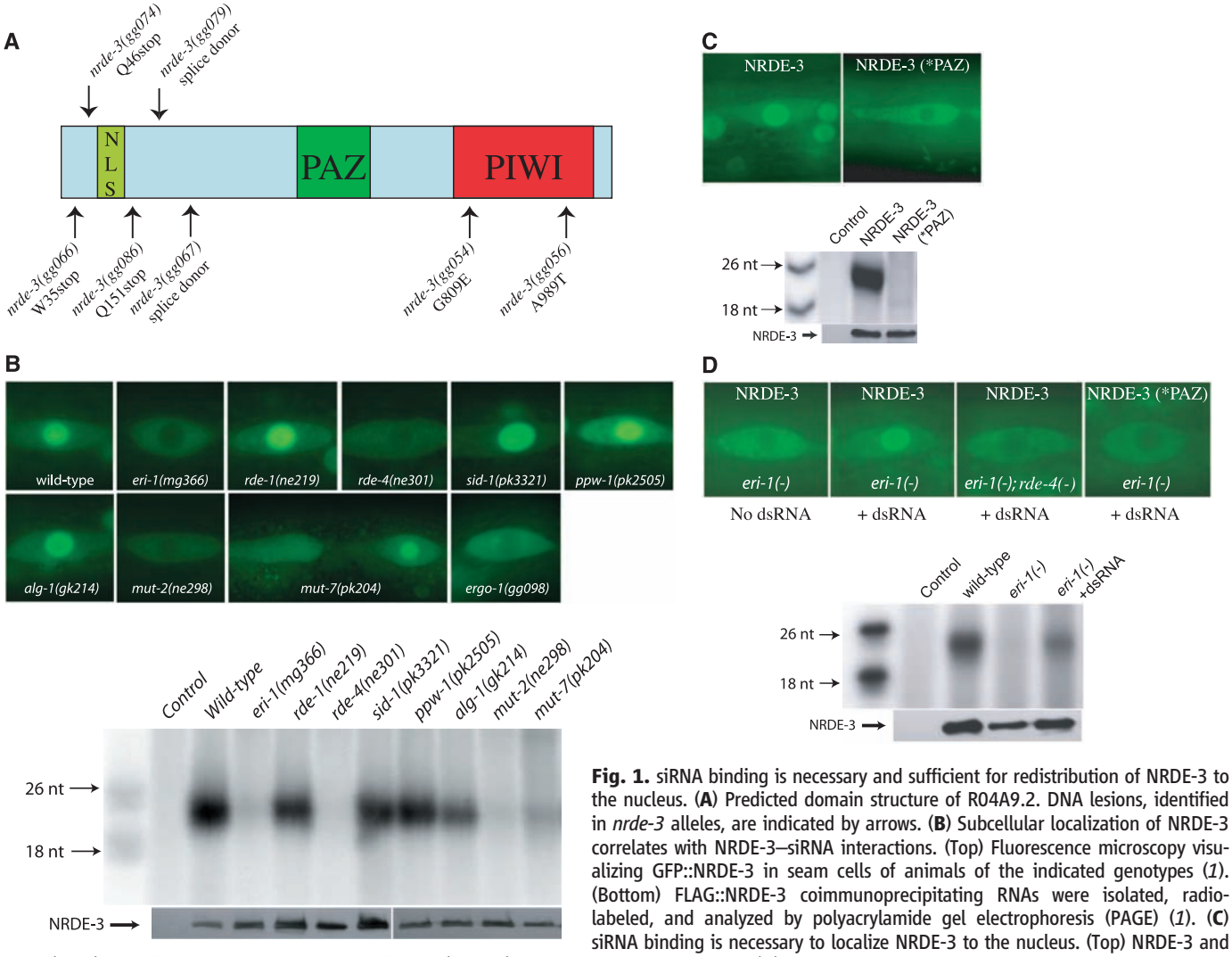

Fig. 1. siRNA binding is necessary and sufficient for redistribution of NRDE-3 to the nucleus. (**A**) Predicted domain structure of R04A9.2. DNA lesions, identified in *nrde-3* alleles, are indicated by arrows. (**B**) Subcellular localization of NRDE-3 correlates with NRDE-3–siRNA interactions. (Top) Fluorescence microscopy visualizing GFP::NRDE-3 in seam cells of animals of the indicated genotypes (*1*). (Bottom) FLAG::NRDE-3 coimmunoprecipitating RNAs were isolated, radiolabeled, and analyzed by polyacrylamide gel electrophoresis (PAGE) (*1*). (**C**) siRNA binding is necessary to localize NRDE-3 to the nucleus. (Top) NRDE-3 and NRDE-3(*PAZ) subcellular localization in seam cells and (bottom) coprecipitating endo siRNAs. (**D**) siRNA binding is sufficient for nuclear redistribution of NRDE-3. (Top) GFP::NRDE-3 localization in seam cells and (bottom) FLAG::NRDE-3 coprecipitating exo siRNAs, in animals lacking endo siRNAs, 36 hours after exposure to control bacteria or dsRNA-expressing bacteria (*1*). (-) indicates superscript minus.

ilar to that of wild-type NRDE-3, which indicated that NRDE-3 interacts with siRNAs in the cytoplasm (Fig. 3C).

Finally, RNAi targeting *lin-15b* and *unc-40* induced an association between NRDE-3 and unspliced *lin-15b* and *unc-40* RNAs, respectively (Fig. 3D and fig. S5A). NRDE-3–pre-mRNA interactions were siRNA-dependent and occurred in the nucleus: NRDE-3(*PAZ) and NRDE-

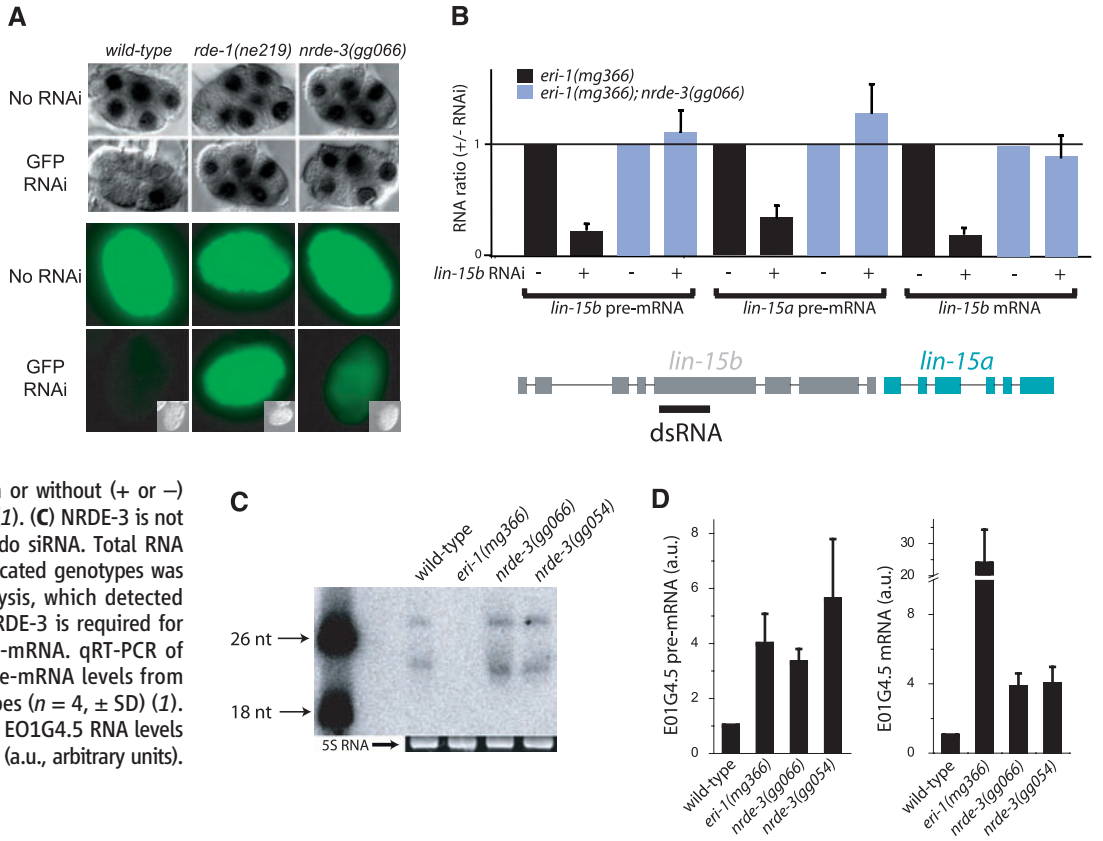

Fig. 2. NRDE-3 is required for nuclear RNAi. (**A**) NRDE-3 is essential for silencing of the nuclear-localized *pes-10::GFP* RNA. (Top) Light microscopy of ~6 cell embryos subjected to in situ hybridization targeting the *pes-10::gfp* RNA with or without GFP dsRNA (*1*). (bottom) Fluorescence microscopy of ~300 cell embryos with or without GFP dsRNA. (**B**) NRDE-3 is required for RNAi-driven silencing of nuclear-localized *lin-15* bicistronic RNA. Quantitative reverse transcriptase polymerase chain reaction (qRT-PCR) analysis of *lin-15a/b* pre-mRNA and *lin-15b* mRNA levels in animals with or without (+ or –) *lin-15b* dsRNA (n = 4 to 8, ± SD) (*1*). (**C**) NRDE-3 is not required for production of an endo siRNA. Total RNA isolated from animals of the indicated genotypes was subjected to Northern blot analysis, which detected E01G4.5 endo siRNAs (*1*). (**D**) NRDE-3 is required for silencing of an endogenous pre-mRNA. qRT-PCR of E01G4.5 mRNA and E01G4.5 pre-mRNA levels from animals of the indicated genotypes (n = 4, ± SD) (*1*). Data are expressed as the ratio of EO1G4.5 RNA levels in wild-type versus mutant animals (a.u., arbitrary units).

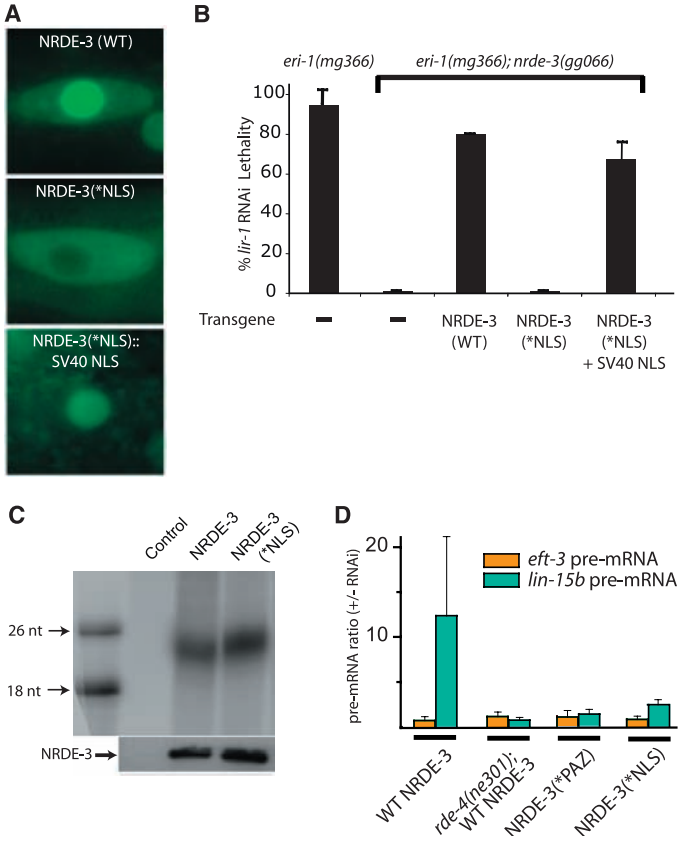

Fig. 3. NRDE-3 transports siRNAs from the cytoplasm to the nucleus: an obligatory step for nuclear RNAi. (**A**) NRDE-3 contains a functional NLS. Fluorescence microscopy of seam cells of animals expressing GFP::NRDE-3 and its variants (*1*). (**B**) Nuclear localization of NRDE-3 is required for nuclear RNAi. *lir-1* RNAi-mediated lethality results from silencing of the nuclear-localized *lir-1–lin-26* polycistronic RNA (*1*, *14*). L1 animals of the indicated genotypes expressing the indicated NRDE-3 variants were fed bacteria expressing *lir-1* dsRNA for 60 hours and scored for viability (n = 3, ± SD). (**C**) NRDE-3 associates with siRNAs in the cytoplasm. FLAG::NRDE-3– and FLAG::NRDE-3 (*NLS)–associated endo siRNAs were purified and labeled as described in Fig. 1B. (**D**) NRDE-3 associates with pre-mRNA in an RNAi-dependent manner. FLAG::NRDE-3 was immunoprecipitated from animals expressing indicated NRDE-3 variants (+/–) exposure to *lin-15b* dsRNA. cDNAs generated from associating RNAs (n = 4, ± SD) were analyzed by qRT-PCR (*1*). Data are expressed as the ratio of coprecipitating *lin-15b* RNA levels (+/–) RNAi. Similar levels of NRDE-3 were immunoprecipitated in each experiment (not shown in figure) and similar results were obtained following *unc-40* RNAi (fig. S5A).

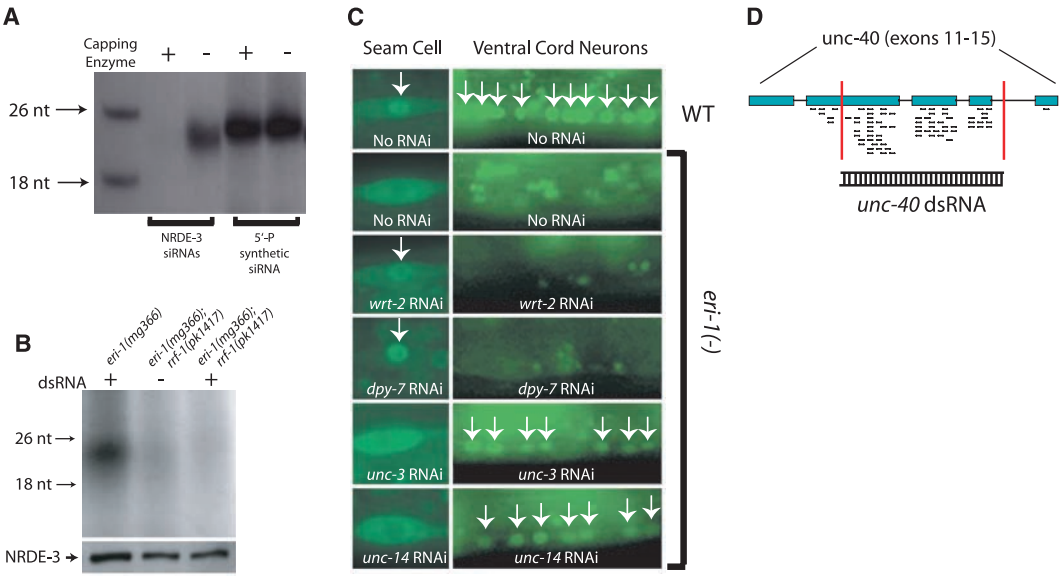

Fig. 4. NRDE-3–associated siRNAs are generated by RdRPs acting on cytoplasmic mRNA targets. (**A**) NRDE-3–associated siRNAs carry 5′ di- or triphosphates. FLAG::NRDE-3–associated endo siRNAs were treated (+) or not (–) with guanylyl transferase and GTP and then detected as described in Fig. 1B. (**B**) Animals of indicated genotypes were fed (+) or not fed (–) bacteria expressing *unc-22* dsRNA for 24 hours, and FLAG::NRDE-3–associated RNAs were detected as described in Fig. 1B. (**C**) *eri-1(mg366)* animals were fed bacteria expressing indicated dsRNAs. After 16 hours, GFP::NRDE-3 localization was assessed. Arrows indicate nuclear localization. (**D**) *eri-1(mg366)* animals were exposed to *unc-40* dsRNA (targeted sequences indicated by vertical red lines), and FLAG::NRDE-3–associated siRNAs were cloned (*1*). Short black lines represent *unc-40* sequences identified.

3(*NLS) failed to associate with pre-mRNA to an extent similar to that of wild-type NRDE-3. RNAi-driven association of NRDE-3 with pre-mRNA is consistent with a role for NRDE-3 in nuclear silencing events and may provide insights into the mechanism of nuclear silencing in *C. elegans*. Taken together, these data indicate that NRDE-3 can escort endo and exo siRNAs from the cytoplasm to the nucleus in an NLS-dependent manner, and that this translocation step is essential for silencing nuclear-localized RNAs.

NRDE-3 is required for silencing E01G4.5 pre-mRNA, but only partially required for endogenous RNAi-mediated silencing of E01G4.5 mRNA, which suggests that NRDE-3 may not be required for cytoplasmic silencing events (Fig. 2D). Three lines of evidence support this hypothesis. First, expression of NRDE-3(*NLS) did not enhance RNAi responses: *nrde-3*$^{-}$, as well as *nrde-3*$^{-}$ animals expressing NRDE-3(*NLS), responded similarly to RNAi (fig. S5, B and C). Second, *nrde-3*$^{-}$ animals retained the ability to respond (albeit at somewhat attenuated levels) to RNAi targeting RNAs (such as *pos-1*, *unc-22*, *unc-15*, *unc-73*, and *dpy-13*) not localized exclusively to the nucleus (Table 1). Incidentally, the near–wild-type response of *nrde-3*$^{-}$ animals to these dsRNAs indicates that (for unknown reasons) NRDE-3–dependent silencing is not always a significant component of RNAi responses after typical feeding RNAi experiments in *C. elegans*. Finally, at the >16-cell stage of embryonic development, the *pes-10::GFP* RNA is transported to the cytoplasm (*9*). Late stage (~300-cell) *nrde-3*$^{-}$ embryos, exposed to GFP dsRNA, retained the ability to partially silence PES-10::GFP (Fig. 2A, bottom). Thus, whereas NRDE-3 is required for RNAi of nuclear-localized RNAs, it is not required for all RNAi-related silencing events and likely does not play a significant role in silencing of cytoplasmic mRNAs.

We next examined NRDE-3–associated siRNAs in more detail. About 85% of NRDE-3–associated siRNAs are substrates for in vitro RNA capping reactions catalyzed by guanylyl transferase, indicating that NRDE-3–associated siRNAs carry 5′ di- or triphosphates (Fig. 4A). RNA-dependent RNA polymerases (RdRPs) are thought to amplify RNAi signals by utilizing RNA molecules, which have been targeted by RNAi, as templates for transcription of additional siRNAs. The presence of 5′ di- or triphosphates on NRDE-3–associated siRNAs suggested that these siRNAs might be generated by RdRP action (*15*, *16*). Three lines of evidence support this hypothesis. First, the RdRP, RRF-1 was required for silencing of the *lir-1–lin-26* polycistronic RNA in response to *lir-1* RNAi (Table 1). In addition, in *rrf-1*$^{-}$ animals NRDE-3 failed to associate with exo siRNAs after RNAi (Fig. 4B). Second, acute exposure (16 hours) of animals lacking endo siRNAs to dsRNAs targeting *wrt-2* and *dpy-7*, two genes expressed in hypodermal cells, triggered a nuclear redistribution of NRDE-3 in hypodermal cells, but failed to initiate NRDE-3 translocation in nonhypodermal cells (Fig. 4C). RNAi targeting *unc-14* and *unc-3*, two genes expressed in ventral cord neurons, triggered NRDE-3 redistribution predominantly in ventral cord neurons (Fig. 4C). Thus, nuclear redistribution of NRDE-3 appears to require expression of RNA molecules exhibiting sequence similarity to the trigger dsRNA (*1*). Third, exposure of animals lacking endo siRNAs to dsRNA targeting the *unc-40* gene induced association of NRDE-3 with siRNAs that are exclusively antisense to the *unc-40* mRNA. Of these siRNAs, 10% were derived from *unc-40* sequences not covered by the *unc-40* dsRNA to which the animals were exposed (Fig. 4D). NRDE-3 associated with *unc-40* siRNAs that exhibited complementarity exclusively to *unc-40* exonic sequences despite the fact that both exonic (82%) and intronic (18%) *unc-40* sequences were targeted by RNAi in these experiments (Fig. 4D). A similar bias toward exonic sequences was observed in NRDE-3–associated endo siRNAs (table S1). These data, in conjunction with our data demonstrating that NRDE-3 associates with siRNAs in the cytoplasm, strongly suggest that NRDE-3 associates predominantly with siRNAs generated by RdRPs acting on mRNA templates in the cytoplasm and that this association is essential for nuclear RNAi.

Our data show that nuclear silencing events in *C. elegans* are the result of transport of siRNAs, and not long dsRNAs, to the nucleus via an active transport system involving Argonaute proteins. *nrde-3*$^{-}$ animals are defective for all nuclear silencing phenomena that we have assayed, which indicates that other mechanisms of siRNA nuclear localization, such as passive diffusion, and/or nuclear envelope breakdown during mitosis are unlikely to be major contributors to these processes. Many small regulatory RNAs, such as scanRNAs in ciliated protozoa, heterochromatin-related siRNAs in plants and fungi, and piRNAs in mammals, are thought to function, at least in part, within the nucleus (*17*–*20*). It will be interesting to determine whether these small regulatory RNAs are transported to the nucleus by mechanisms similar to the one described here.

References and Notes

1. Materials and methods are available as supporting material on *Science* Online.
2. E. Yigit *et al.*, *Cell* **127**, 747 (2006).
3. Single-letter abbreviations for the amino acid residues are as follows: A, Ala; C, Cys; D, Asp; E, Glu; F, Phe; G, Gly; H, His; I, Ile; K, Lys; L, Leu; M, Met; N, Asn; P, Pro; Q, Gln; R, Arg; S, Ser; T, Thr; V, Val; W, Trp; and Y, Tyr.
4. R. C. Lee, C. M. Hammell, V. Ambros, *RNA* **12**, 589 (2006).
5. T. F. Duchaine *et al.*, *Cell* **124**, 343 (2006).
6. J. J. Song, S. K. Smith, G. J. Hannon, L. Joshua-Tor, *Science* **305**, 1434 (2004).
7. J. B. Ma, K. Ye, D. J. Patel, *Nature* **429**, 318 (2004).
8. H. Tabara, E. Yigit, H. Siomi, C. C. Mello, *Cell* **109**, 861 (2002).

9. M. K. Montgomery, S. Xu, A. Fire, *Proc. Natl. Acad. Sci. U.S.A.* **95**, 15502 (1998).
10. T. Blumenthal *et al.*, *Nature* **417**, 851 (2002).
11. S. G. Clark, X. Lu, H. R. Horvitz, *Genetics* **137**, 987 (1994).
12. L. S. Huang, P. Tzou, P. W. Sternberg, *Mol. Biol. Cell* **5**, 395 (1994).
13. S. Kennedy, D. Wang, G. Ruvkun, *Nature* **427**, 645 (2004).
14. J. M. Bosher, P. Dufourcq, S. Sookhareea, M. Labouesse, *Genetics* **153**, 1245 (1999).
15. J. Pak, A. Fire, *Science* **315**, 241 (2007).
16. T. Sijen, F. A. Steiner, K. L. Thijssen, R. H. Plasterk, *Science* **315**, 244 (2007).
17. I. M. Hall *et al.*, *Science* **297**, 2232 (2002).
18. T. A. Volpe *et al.*, *Science* **297**, 1833 (2002).
19. K. Mochizuki, N. A. Fine, T. Fujisawa, M. A. Gorovsky, *Cell* **110**, 689 (2002).
20. M. A. Carmell *et al.*, *Dev. Cell* **12**, 503 (2007).
21. We thank C. Hunter for suggesting utilizing the *pes-10::GFP* strain; J. Kimble for use of confocal microscope; P. Anderson, D. Wassarman, J. Dahlberg, and E. Lund for comments; and the *Caenorhabditis* Genetics Center for strains. This work was supported by grants from the Pew and Shaw scholars programs, NIH, and the American Heart Association.

Supporting Online Material

www.sciencemag.org/cgi/content/full/321/5888/537/DC1
Materials and Methods
Figs. S1 to S5
Table S1
References

11 March 2008; accepted 28 May 2008
10.1126/science.1157647

Entangling the Spatial Properties of Laser Beams

Katherine Wagner,[1] Jiri Janousek,[1] Vincent Delaubert,[1,2] Hongxin Zou,[1] Charles Harb,[3] Nicolas Treps,[2] Jean François Morizur,[1,2] Ping Koy Lam,[1] Hans A. Bachor[1]*

Position and momentum were the first pair of conjugate observables explicitly used to illustrate the intricacy of quantum mechanics. We have extended position and momentum entanglement to bright optical beams. Applications in optical metrology and interferometry require the continuous measurement of laser beams, with the accuracy fundamentally limited by the uncertainty principle. Techniques based on spatial entanglement of the beams could overcome this limit, and high-quality entanglement is required. We report a value of 0.51 for inseparability and 0.62 for the Einstein-Podolsky-Rosen criterion, both normalized to a classical limit of 1. These results are a conclusive optical demonstration of macroscopic position and momentum quantum entanglement and also confirm that the resources for spatial multimode protocols are available.

Position and momentum are a fundamental example of conjugate quantum observables. Optical measurements of this conjugate pair are ubiquitous throughout many fields of research and across a broad range of scales. Applications in optics span from biology to astronomy, from the nanometer regime with atomic force microscopy (*1*) and optical tweezing (*2*) to the kilometer regime with free-space optical communication (*3*) and interferometry (*4*, *5*). These applications require continuous sampling of the data, although their accuracy is fundamentally limited by the quantum noise of these beams. Special squeezed beams, with the noise suppressed in one quadrature, have been used to improve the properties of many optical instruments (*6*), improving the signal-to-noise ratio for one selected observable.

Quantum entanglement, where two systems are quantum-correlated, can allow a near-perfect prediction from one system to the other and can enable new techniques for using information from one system to act on the other, thereby overcoming the limits set by quantum noise. In optics the systems are beams of light, with a single mode of electromagnetic radiation describing all their properties. Each beam can be represented by a single quantum operator. Such single-mode continuous wave (CW) optical beams have already been used to demonstrate strong entanglement between the amplitude and phase quadrature of pairs of beams (*7*–*9*) or the polarization of the beams (*10*–*13*). In combination with feed-forward control, these beams can be used for applications such as entanglement distillation (*14*) and teleportation (*15*).

However, laser beams have additional spatial properties that are described by higher-order spatial modes. A multimode description contains more information and allows the coding of more complex, multidimensional quantum information (*16*). The experimental techniques are direct and reliable because of the link between spatial properties and the well-known basis of Hermite-Gaussian transversely excited laser modes (TEM_{ij}, where i and j are the order numbers in the x and y directions). For a CW beam with the energy in a pure TEM_{00} mode (the reference beam) and detectable power of microwatts to milliwatts, the simplest spatial modulation is a displacement of the entire mode in the transverse directions x and y. For a periodic displacement at a frequency Ω, where the size of the displacement is much smaller than the diameter ω_0 of the beam, all of the information about the displacement $X(\Omega)$ is contained in the real part (or amplitude quadrature) of the mode TEM_{10}, whereas the orthogonal displacement $Y(\Omega)$ appears in the real part of TEM_{01}. The accuracy of the measurement of the position of the beam is limited by quantum noise in the modes TEM_{10} and TEM_{01}. Previously, we have generated squeezed light in these higher-order modes (*17*). This technique of synthesizing is different from the idea of entangling images and complements the generation of intensity using four-wave mixing in an atomic vapor where a large number of modes can be entangled (*18*).

Concentrating on one transverse direction, the displacement X of the beam forms a conjugate pair of observables with the direction θ of the beam. The information for the direction is contained in the imaginary part (or phase quadrature) of the corresponding higher-order mode. This can be seen by the following expression for the electric field distribution $E(X, \theta)$ of a TEM_{00} mode that is both displaced by X and tilted by θ with the spatial information in the TEM_{10} mode (*19*)

$$E(X,\theta) \approx \mathrm{TEM}_{00} + \frac{X}{\omega_0}\mathrm{TEM}_{10} + i\frac{\omega_0\pi\theta}{\lambda}\mathrm{TEM}_{10} \quad (1)$$

where ω_0 is the waist diameter, i is the imaginary unit, and λ is the wavelength of the beam. The direction of the laser beam θ corresponds to the transverse momentum of the photons in the beam. An improvement in the spatial accuracy beyond the quantum noise limit (QNL) for either position or direction measurement of a TEM_{00} beam has already been demonstrated (*6*).

We then investigated the spatial entanglement of a pair of beams (*20*). The existence of entanglement can be determined by measuring correlations between the displacements and directions of the two beams, respectively, to a level below the QNL. For beams that are coherent states, the spatial fluctuations of the two beams A and B are independent, and there are no correlations or anticorrelations. Thus, variance measurements for the sum $V(X_A + X_B)$ and difference $V(X_A - X_B)$ of the positions of the beams are

[1]Australian Research Council Centre of Excellence for Quantum-Atom Optics, Australian National University, Canberra ACT 0200, Australia. [2]Laboratoire Kastler Brossel, Université Pierre et Marie Curie-Paris 6, ENS, CNRS; 4 place Jussieu, 75252 Paris, France. [3]Australian Defence Force Academy, Canberra, Australia.

*To whom correspondence should be addressed. E-mail: hans.bachor@anu.edu.au

ERRATUM

Post date 4 December 2009

Research Article: "An Argonaute transports siRNAs from the cytoplasm to the nucleus" by S. Guang *et al.* (25 July 2008, p. 537). The rightmost four images in the top panel of Fig. 2A and the top image of Fig. 3A were inadvertently mislabeled and duplicated. Investigators who were not involved in the original experiments have repeated these experiments, which yielded results similar to those originally reported. Our conclusions remain unaltered. The corrected figures are shown here.